

High Density n-Si/n-TiO₂ Core/Shell Nanowire Arrays with Enhanced Photoactivity

*Yun Jeong Hwang, Akram Boukai, and Peidong Yang**

Department of Chemistry, University of California, Berkeley, California 94720,

and Material Sciences Division, Lawrence Berkeley National Laboratory, Berkeley, California 94720

RECEIVED DATE (to be automatically inserted after your manuscript is accepted if required according to the journal that you are submitting your paper to)

CORRESPONDING AUTHOR FOOTNOTE

To whom correspondence should be addressed:

Peidong Yang: Email: p_yang@berkeley.edu

ABSTRACT

There are currently great needs to develop low-cost inorganic materials that can efficiently perform solar water splitting as photoelectrolysis of water into hydrogen and oxygen has significant potential to provide clean energy. We investigate the Si/TiO₂ nanowire heterostructures to determine their potential for the photooxidation of water. We observed that highly dense Si/TiO₂ core/shell nanowire arrays enhanced the photocurrent by 2.5 times compared to planar Si/TiO₂ structure due to their low reflectance and high surface area. We also showed that n-Si/n-TiO₂ nanowire arrays exhibited a larger photocurrent and open circuit voltage than p-Si/n-TiO₂ nanowires due to a schottky barrier at the heterojunction.

KEYWORDS: Solar water splitting, Si, TiO₂, heterojunction, core/shell nanowire

MANUSCRIPT TEXT

Direct solar energy conversion to storable fuels such as hydrogen offers a promising route towards less reliance on fossil fuels.¹⁻⁴ For example, photoelectrolysis of water to generate H₂ on a semiconductor/electrolyte interface has the attractive advantages of clean processing and energy savings over steam reforming of natural gas. One of the most critical issues in solar water splitting is the development of a photoanode with high efficiency and long term durability in an aqueous environment. TiO₂ has been extensively studied as a photoanode due to its high resistance to photocorrosion.⁵⁻¹⁰ However, its conversion efficiency of solar energy to hydrogen is still low (less than 4 %)⁶ due to its large bandgap (3.0 ~3.2 eV). TiO₂ requires an external bias to reduce water for H₂ production to overcome the chemical over potential.^{5, 11} Si (E_g = 1.12 eV), on the other hand, can absorb sunlight efficiently. It is however challenging to use Si for photoelectrolysis since it readily corrodes in water. Moreover, it is thermodynamically impossible for Si to oxidize water spontaneously due to its high

valence band maximum (VBM) energy. Therefore, a composite semiconductor electrode composed of a semiconductor heterojunction has been proposed to compensate these shortcomings. In these cases, the photoanode is composed of a small band gap semiconductor that is protected by a stable semiconductor.¹²⁻¹⁴

Semiconductor heterojunctions can absorb different region of the solar spectrum.¹⁵⁻¹⁸ The advantage of composite structures is that each semiconductor need to satisfy one energetic requirement: matching the conduction band minimum (CBM) or VBM with either the H₂ reduction or O₂ oxidation potential. Single semiconductor materials typically can not satisfy the requirements of suitable bandgap energies for efficient solar absorption and meantime with band-edges aligned with both the H₂ and O₂ redox potential of water.^{3,19} Here, we prepared TiO₂ coated Si nanowire arrays and studied their photo-oxidative properties. We observed that Si/TiO₂ core/shell nanowire arrays showed higher photocurrent than the planar Si/TiO₂. A semiconductor heterojunction of n-Si/n-TiO₂ or p-Si/n-TiO₂ has different band bending properties near the junction.^{12, 20} The n/n heterojunction has a potential energy barrier between the two semiconductor regions that reflects minority holes in the TiO₂ similar to the back surface field in solar cell.²¹ Using photocurrent and open circuit voltage measurements, we show that the n/n heterojunction is more promising for photoelectrochemical (PEC) cell application.

Highly oriented Si nanowire arrays on the silicon wafers were synthesized by an aqueous electroless etching method.²² These Si nanowire arrays significantly suppress reflection which has the potential to provide a higher efficiency of PEC cell. We prepared n-type and p-type Si electroless etched nanowire (EENW) arrays from n-Si(100) (P doped, 0.6~0.8 Ωcm) and p-Si(100) (B doped, 1~5 Ωcm) wafers with dopant concentrations of $\sim 10^{16}$ cm⁻³. A clean silicon wafer was immersed into the etching solution containing 0.04 M AgNO₃ (99.999%, Aldrich) and 5M HF (49%, Honeywell) at room temperature. The length of the EENW was controlled by the etching time (0.2 μm/min growth rate).

TiO₂ was grown both on the Si EENW arrays and the planar Si wafer by a home-built atomic layer deposition (ALD) system with TiCl₄ (99.990%, Alfa) and pure water as the precursors. Si samples were cleaned with a buffered HF solution to remove the native oxide layer right before loading into the ALD

vacuum chamber. The ALD system deposits polycrystalline anatase TiO₂ layer with an average growth rate of 1.2 Å per cycle on the planar Si wafer and 0.7 Å per cycle on our Si EENW arrays at 300 °C. On the Si EENW array, diffusion of the gas precursors is reduced due to the high density of the nanowire arrays, which leads to slower growth rate than the planar substrate. Care was taken to ensure that the TiO₂ thickness on the EENW arrays and planar substrates were equivalent.

Typical cross sectional scanning electron microscope (SEM) and the transmission electron microscope (TEM) images of Si EENW and the ALD TiO₂ coated Si EENW (Si EENW/TiO₂) are shown in Figure 1a-d. The Si EENW and Si EENW/TiO₂ arrays are produced vertically on the Si wafer with high density. Si EENW maintains the same crystallinity as the starting Si wafer,²² and their diameters are in the range of 20 ~ 200 nm. Figure 1d shows polycrystalline TiO₂ deposition on the EENW. Figure 1e and f show the top view SEM images of Si EENW/TiO₂ arrays and TiO₂ thin film on the Si(100) wafer with average thickness of 35 nm. The nanocrystalline nature of the TiO₂ coating is similar for deposition on the nanowire surface and on the flat wafer surface. The X-ray diffraction (XRD) characterization indicates that the ALD grown TiO₂ layer has an anatase structure both on the Si(100) wafer and on the Si EENW array, as shown in Figure 2. For photoelectrolysis of water, anatase TiO₂ has the advantage of a flat band potential (U_{fb}) that is 200 mV more negative than that of the rutile TiO₂. This allows anatase TiO₂ to have sufficient cathodic potential for hydrogen reduction from water.²³ The carrier concentration (N_D) of TiO₂ layer by ALD was determined by capacitance versus voltage measurement. 90 nm TiO₂ thin film was deposited on the highly doped n-Si wafer (As doped, 0.001~0.004 Ωcm), and Ni was deposited on the TiO₂ thin film. From the Mott-Schottky relation, N_D was found to be $2.76 \times 10^{17} \text{ cm}^{-3}$. The TiO₂ becomes n-type semiconductor because of defects such as oxygen vacancies and titanium interstitials, and their carrier concentration varies from $\sim 10^{17} \text{ cm}^{-3}$ to $\sim 10^{20} \text{ cm}^{-3}$ depending on synthesis.²⁴⁻²⁶

Photocurrent measurements were performed in a 1M KOH electrolyte with three electrodes configuration (EG&E Pinceton Applied Research Potentiostat, VersaStat II): Si/TiO₂ photoanode as a working electrode, Pt gauze as a counter electrode, and a saturated calomel electrode (SCE, Pine

Research Instrumentations, AFREF1) as a reference electrode. All three electrodes are in a glass cell which has a 1 inch quartz window, and Ar gas was bubbled through to remove the dissolved oxygen during the measurement. The current versus potential measurements were carried out at a 10 mV/s sweep rate. A constant light intensity of 100mW/cm² from a 450 W Xe lamp (Oriel, 6266) illuminated our samples, and a liquid filter (Oriel, 6123NS) was used to avoid solution heating by infrared light.

Figure 3a shows the photocurrent versus bias potential characteristics for Si/TiO₂ composite photoanodes. Under illumination, oxidation of water takes place on the photoanode.



The photocurrent versus bias potential curves have three regions: low photocurrent density region at negative bias potential (region I), plateau of the photocurrent density at more positive bias potential (region III), and increasing photocurrent density region (region II) between regions I and III. No photocurrent passes through the semiconductor and electrolyte interface when the negative bias voltage is close to the flat band potential because any created excess holes and electrons are recombined before holes transfer into the electrolyte (region I).²⁷ The photocurrent plateau appears as the bias potential sweeps to more positive direction (region III), where the photocurrent is limited by the number of the holes excited by illumination.

Our planar Si/TiO₂ samples show comparable photocurrent density to those reported in the literature. The reported value⁹ for a 15 μm thick film of P-25 TiO₂ on Ti foil is 0.1 mA/cm² under the same illumination conditions (Xe lamp, 100 mW/cm²) even though the thickness of our ALD grown TiO₂ film is only 35 nm. At region III, 20 μm long Si EENW/TiO₂ samples show 2.5 times higher photocurrent density than planar Si/TiO₂ samples for both n-type and p-type Si. The Si EENW/TiO₂ composites have higher photocurrent mainly because of lower reflectance and larger surface area than the Si planar/TiO₂.

Figure 3a also shows that n-Si/n-TiO₂ composites have 20~25 % higher photocurrent density and more negative onset potential than those of p-Si/n-TiO₂ for both nanowire and planar structures. Higher photocurrent is expected for the n/n junction since band bending at the junction helps charge separation.

The band bending of the semiconductors at the junctions were shown in Figure 3b and c. The Fermi energy (E_F) of our n and p type silicon are -4.25 eV, and -4.97 eV (relative to the vacuum level), respectively. E_F of TiO_2 was calculated²⁸⁻²⁹ from the reported electron effective mass in anatase ($m_e^* = 1m_e$)³⁰ and the measured carrier concentration ($N_D = 2.76 \times 10^{17} \text{ cm}^{-3}$). Figure 3b illustrates the charge flow in n-Si/n- TiO_2 junctions under illumination. The e^-/h^+ pairs are created inside both the Si and TiO_2 because the TiO_2 shell is transparent under visible light. Visible light can be harvested by the core Si. Under the illumination, Fermi energies of the electrons and holes, so-called quasi-Fermi energies (E_F^*), differ from E_F in dark,¹⁹ and the quasi Fermi energies of minority holes (${}_pE_F^*$) in the n-Si and n- TiO_2 are shown. The photogenerated hole in TiO_2 (${}_{TiO_2}h^+$) moves toward the n- TiO_2 /electrolyte interface and oxidizes OH^- to oxygen, while photogenerated electrons in the n- TiO_2 (${}_{TiO_2}e^-$) move away from the front surface due to the schottky barrier at the interface with the electrolyte.

In addition to this charge separation, the interface between the n-Si and n- TiO_2 reduces the loss of holes in the TiO_2 region which results in an increase of the photoanodic current. The potential barrier seen by the holes at the n-Si/n- TiO_2 junction reflects holes back into the TiO_2 layer (Figure 3b). This is analogous to the back surface field of a solar cell which has shown larger photocurrent and larger output voltage by adding a heavily doped region adjacent to the contact.³¹ To complete the circuit, the photogenerated electrons in the n-Si (${}_{Si}e^-$) move to the counter electrode where the reduction reaction takes place. The photogenerated hole in n-Si (${}_{Si}h^+$) moves toward the n-Si/n- TiO_2 junction and recombines with the ${}_{TiO_2}e^-$. Therefore, n-Si/n- TiO_2 core/shell structure shows the largest increase in photocurrent since its band alignment at the junction helps reduce recombination under illumination. In the case of p-Si/n- TiO_2 junctions, the flow of electrons and holes at the junction of p-Si/n- TiO_2 is opposite to the desirable direction. Figure 3c shows that ${}_{TiO_2}h^+$ can move either to the electrolyte or to the p-Si in p/n junction. The p-Si/n- TiO_2 junction, therefore, has smaller observed photo-anodic current density than n-Si/n- TiO_2 .

The larger photocurrent in the n-Si/n-TiO₂ leads to a larger negative onset potential. This is a result of the n/n junction's effective charge separation that leads to a larger short circuit current (J_{sc}).³¹ Both n-Si EENW/TiO₂ and p-Si EENW/TiO₂ have similar dark current values (5 μ A/cm²). Also, higher V_{oc} is expected for n-Si/n-TiO₂ since the E_F and band energies of the n-Si and n-TiO₂ shift upward at open circuit under the illumination. The V_{oc} of n-Si/n-TiO₂ photoanode is $V_{oc} = V_{oc}(\text{TiO}_2/\text{electrolyte}) + V_{oc}(\text{Si}/\text{TiO}_2)$.²⁰ For the p-Si/n-TiO₂, the band energies of the n-TiO₂ shift upward but the band energies of the p-Si shift downward. The photovoltage at the p-Si/n-TiO₂ junction is in the opposite direction to the photovoltage at the n-TiO₂/electrolyte interface due to the downward band bending. The V_{oc} of p-Si/n-TiO₂ photoanode is $V_{oc} = V_{oc}(\text{TiO}_2/\text{electrolyte}) - V_{oc}(\text{Si}/\text{TiO}_2)$.

We can take the advantage of the higher V_{oc} of the n/n junction for the PEC cell. Enhanced J_{sc} and V_{oc} will provide a higher efficiency PEC cell. Also, for the solar water splitting, larger V_{oc} provides high enough cathodic potential to reduce the water to hydrogen. It is important that the flat band potential of the semiconductor is lower than the hydrogen reduction potential. For example, Fe₂O₃ ($E_g = 2.1$ eV) and WO₃ ($E_g = 2.6$ eV) have been studied due to higher stability and lower band gap than TiO₂. However, both need an external bias voltage to complete the water splitting since their CBMs are lower than hydrogen reduction potential by 0.2 V and 0.1V.⁶ Therefore, the n/n composites have the potential for the spontaneous photoelectrolysis of water.

Stability is another important requirement for the PEC cell. By coating the Si with TiO₂, we can make the photoanode stable in the 1M KOH aqueous solution. The n and p type Si EENW/TiO₂ core/shell structures have shown constant photocurrent levels while testing for one hour (Supporting information Figure S1). In contrast, planar Si wafers and Si EENW arrays generate vigorous H₂(g) bubbles in the KOH electrolyte and as a result they are etched.

Figure 4 demonstrates the photocurrent density depending on the length of the n-Si EENW/TiO₂ arrays. We prepared 5 μ m, 10 μ m, and 20 μ m long n-type Si EENW/TiO₂ arrays and planar n-Si/TiO₂. We observed that the longer Si EENW/TiO₂ arrays have higher photocurrent although the photocurrent density normalized by the length of the nanowires decrease as shown in Figure 4b. All of the three Si

EENW/TiO₂ arrays had significantly lower reflectance than Si planar/TiO₂ sample (supporting information Figure S2). The Si EENW/TiO₂ sample can effectively trap the light by extending the path length due to multiple reflection in a high density array structures similar to textured surfaces.³² When the wires are 5 ~ 20 μm long, their reflectance values are nearly the same. All of the three different length Si EENW/TiO₂ arrays have about 1~2 % of reflectance in the UV region (200~350 nm), and about 5 % of reflectance in the visible region (450 ~900 nm). In addition to low reflectance, the high surface area of Si EENW is also expected to contribute the higher photocurrent since it increases the interface area with the electrolyte as well as the overall amount of TiO₂. Lower reflectance and higher surface area of the Si EENW/TiO₂ contribute to higher absorption and higher photocurrent density than the planar samples.

In order to ascertain the contribution of the core Si, we measured the photocurrent and V_{oc} of the Si/TiO₂ photoanodes under the visible light illumination. The light was passed through a 441.6 nm edge filter to cut off the UV region from the Xe lamp so that carriers are generated only in the Si. We observed that there was no photocurrent under the visible light for all Si/TiO₂ composites. Photogenerated holes in Si cannot be transferred to the valence band of TiO₂ since there is a significant barrier at the junction (Figure 5c and d). Instead, the photogenerated e⁻/h⁺ pairs in the Si recombine so that there is no net charge flux.^{19, 33} Therefore, photo-oxidation cannot take place at the TiO₂ surface unless carriers are photogenerated in the TiO₂ shell.

The V_{oc} shifts under visible light illumination as shown in Figure 5a and b. For n-Si/n-TiO₂, the photogenerated holes in the Si move toward the TiO₂ and recombine with electrons in TiO₂ due to an electric field in space charge region. The charge separation shifts the E_f and the band energies of the n-Si upward, so that the space charge region diminishes. When flat band is attained, there will be no more charge separation. Therefore, the V_{oc} of the n-Si/n-TiO₂ photoanode becomes more negative (Figure 5a). For p-Si/n-TiO₂, the band bending of the p-Si diminishes similar to n-Si/n-TiO₂, but the reduced band bending shifts the band energies of p-Si downward which reduces the V_{oc} under visible light (Figure 5b).

From the change of the V_{oc} under visible light, we confirmed that the core Si absorbs the visible light and it contributes shift of the band energies.

In conclusion, we compared the photocurrent density of the planar Si and Si EENW coated by ALD TiO_2 thin film. The Si EENW/ TiO_2 has 2.5 times higher photocurrent density than the planar Si/ TiO_2 due to lower reflectance and higher surface area. We also observed an increase of the photocurrent by using n-Si/n- TiO_2 heterojunctions because n/n junctions enhance the charge separation and minimize recombination. The n/n heterojunction is a promising structure for solar water splitting since the photovoltage at the junction can compensate the lower energy level of the conduction band of the shell semiconductor. Also, the n/n heterojunction could potentially increase the efficiency of the photovoltaic cell due to a higher open circuit voltage and higher photocurrent.

ACKNOWLEDGMENT This work was supported by the Director, Office of Basic Energy Sciences, Chemical Sciences, Materials Sciences and Engineering Division, of the U.S. Department of Energy under Contract No. DE-AC02-05CH1123. We thank Prof. Nate Lewis and his group for helpful discussion and assistance in the initial testing of our samples.

Supporting Information Available. This material is available free of charge via the Internet at <http://pubs.acs.org>.

FIGURE CAPTIONS (Word Style “VA_Figure_Caption”).

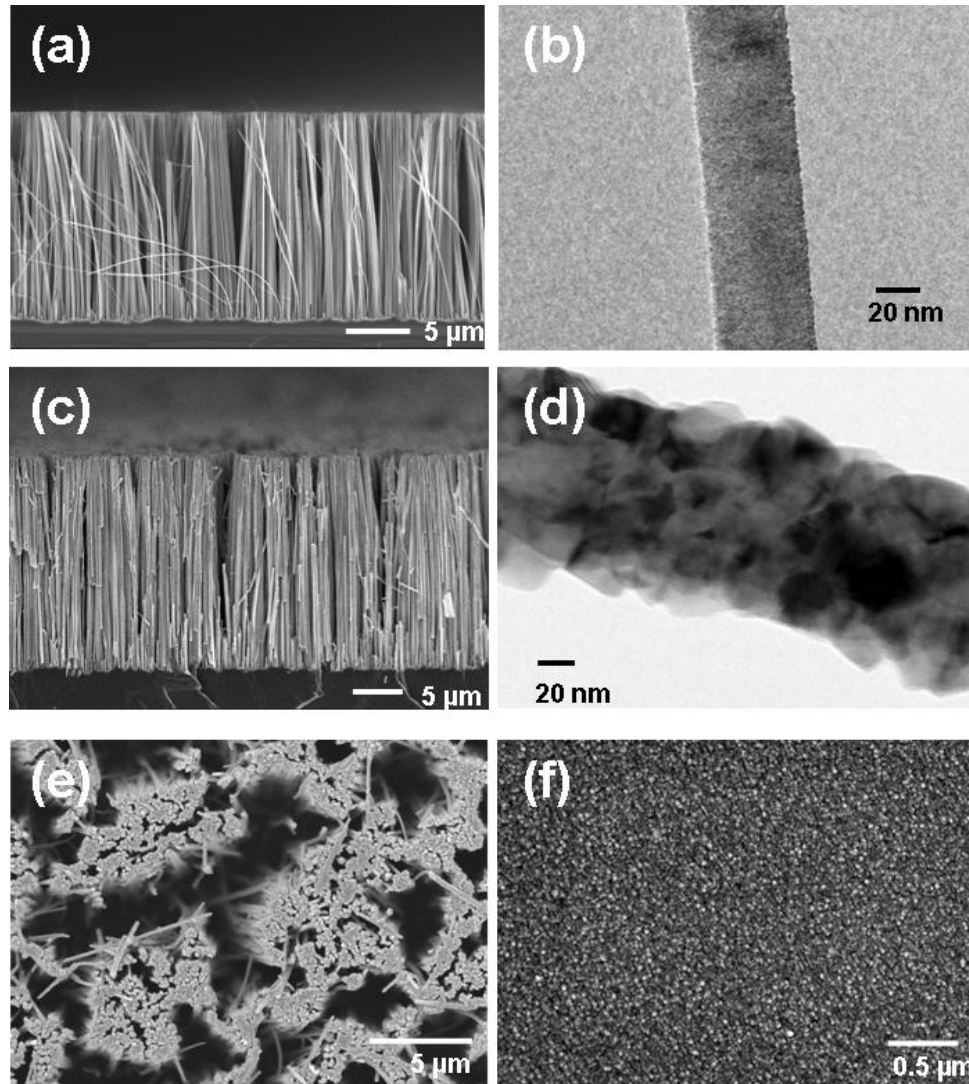


Figure 1. Characterization of Si EENW and Si/TiO₂ core/shell structures. (a) Cross sectional SEM of 20 μm long Si EENW arrays, demonstrating vertical alignment and high density. (b) Typical TEM image of a Si EENW. (c) Cross sectional SEM images of Si EENW arrays coated with TiO₂ by ALD at 300 °C. (d) Typical TEM image of Si EENW/TiO₂ core/shell nanowire, showing that polycrystalline TiO₂ covers the Si EENW. (e) Top view SEM images of Si EENW/TiO₂ array. (f) Top view SEM image an ALD grown TiO₂ thin film on a Si wafer, showing nanometer size grains of TiO₂.

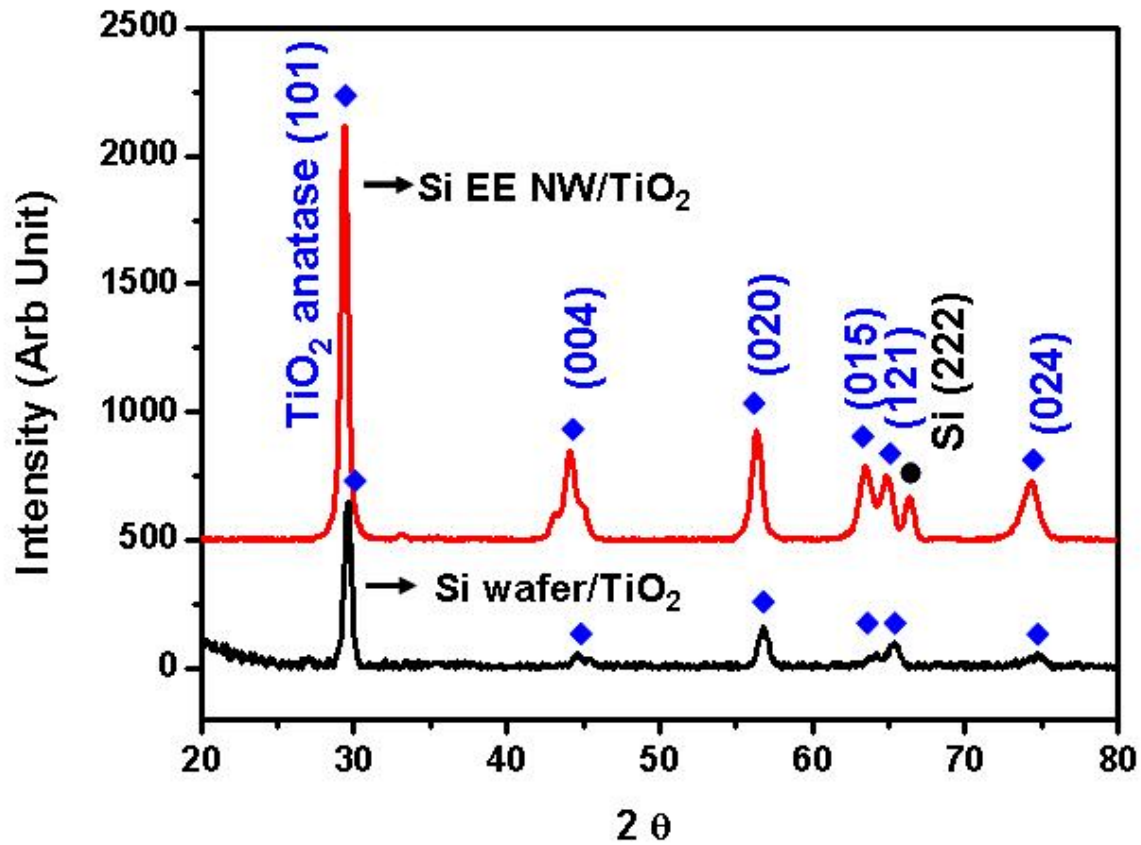


Figure 2. X-ray diffraction pattern of TiO₂ layer grown by ALD at 300 °C. 25~40 nm TiO₂ deposited on Si EENW arrays (red line), 35 nm TiO₂ thin film on a Si planar substrate (black line). Both TiO₂ layers index to polycrystalline anatase.

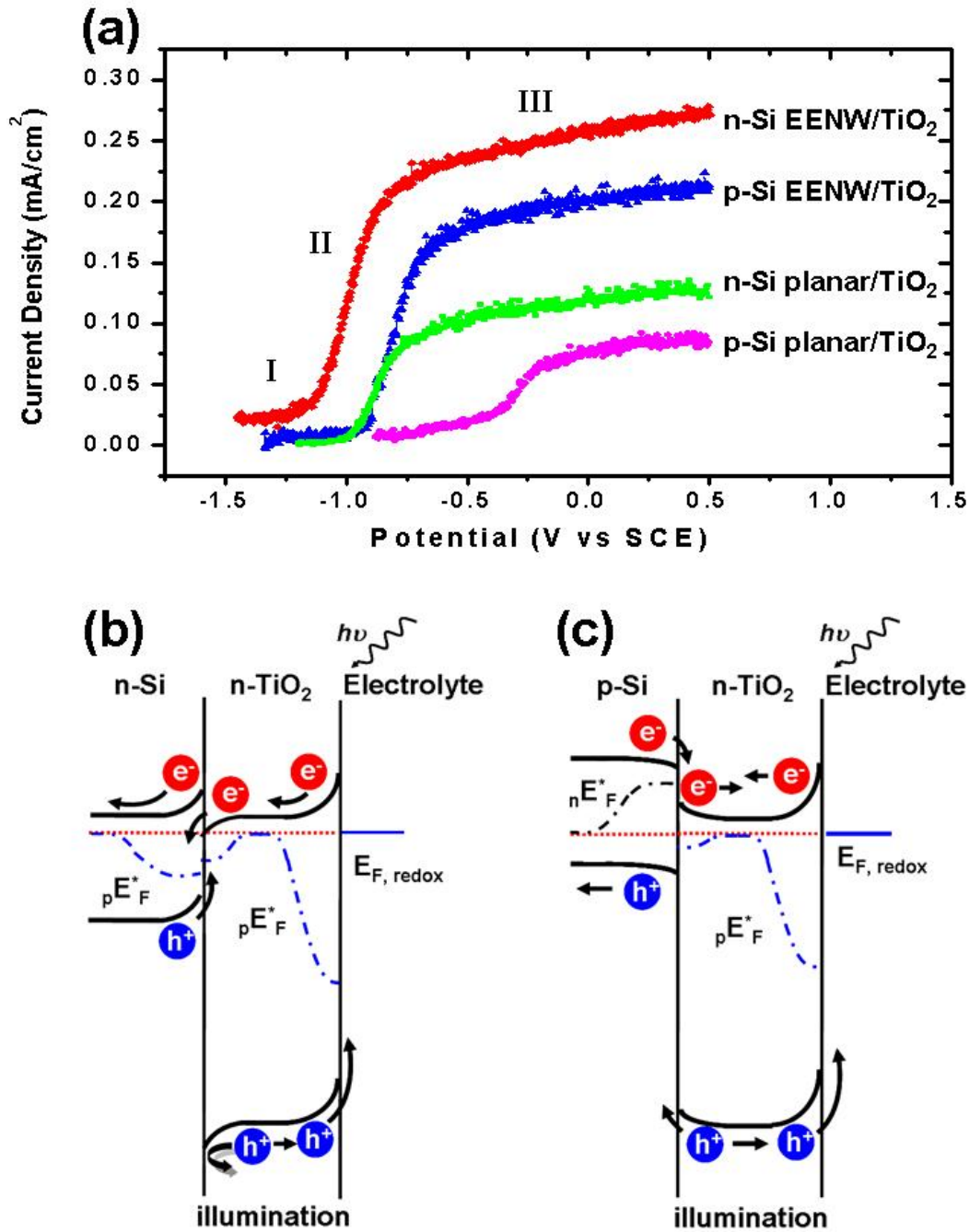


Figure 3. (a) Photocurrent density versus bias potential (vs SCE) of Si/TiO₂ photoanodes: n-Si EENW array coated by TiO₂ (red), p-Si EENW array coated by TiO₂ (blue), n-Si(100) planar substrate coated by TiO₂ (green), p-Si(100) planar substrate coated by TiO₂ (purple). Schematic representation of band energies and charge transfer (b) for n-Si/n-TiO₂ and (c) for p-Si/n-TiO₂ under the illumination. Si EENW/TiO₂ samples have 2.5 times larger photocurrent density than Si planar/TiO₂. n-Si/n-TiO₂ photoanodes have more negative onset potential than p-Si/n-TiO₂ both for planar and nanowire structures.

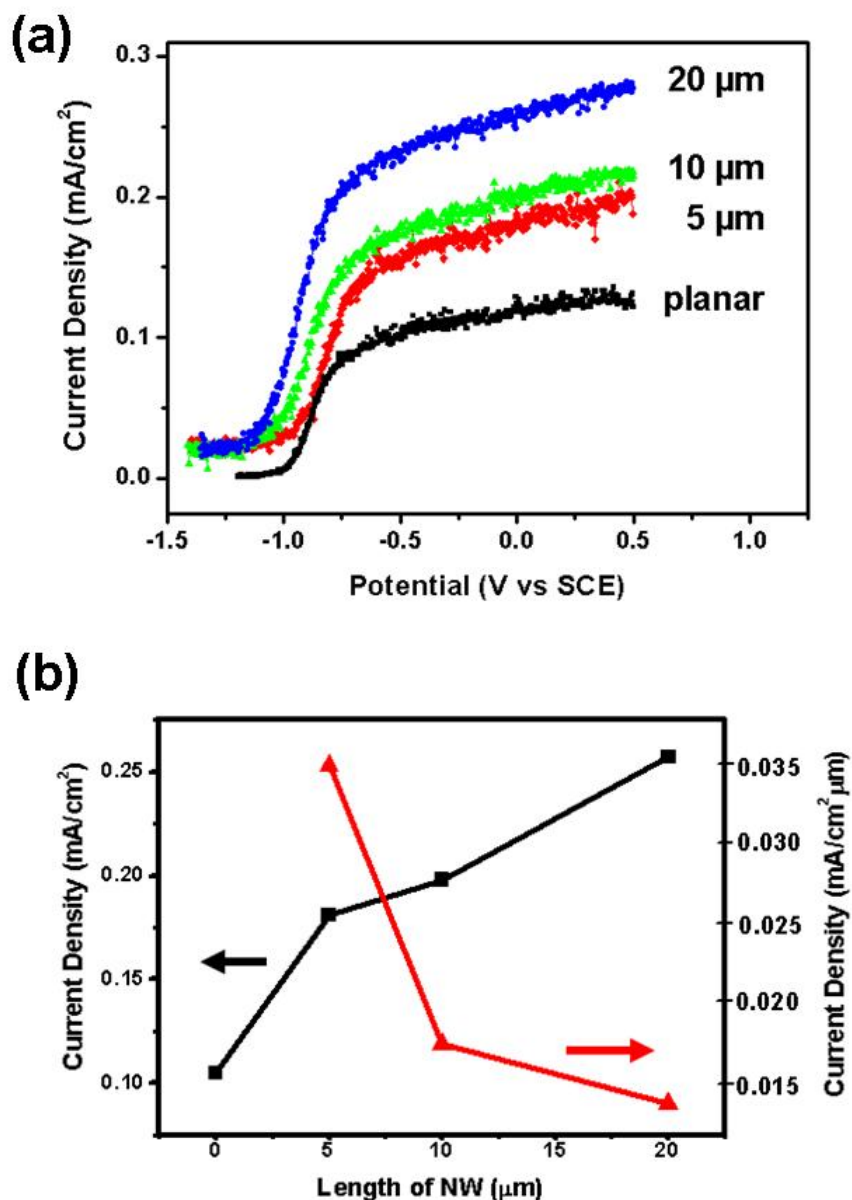


Figure 4. (a) Variation of photocurrent density versus potential depending on the length of n-Si EENW/TiO₂ arrays: 20 μm (blue line), 10 μm (green line), 5 μm (red line) long NW arrays and n-Si planar/TiO₂ (black line). (b) Relationship between photocurrent density versus the length of n-Si EENW/TiO₂, illustrating longer wire arrays have higher photocurrent. The axis to the right is the current density normalized by the length of the nanowire.

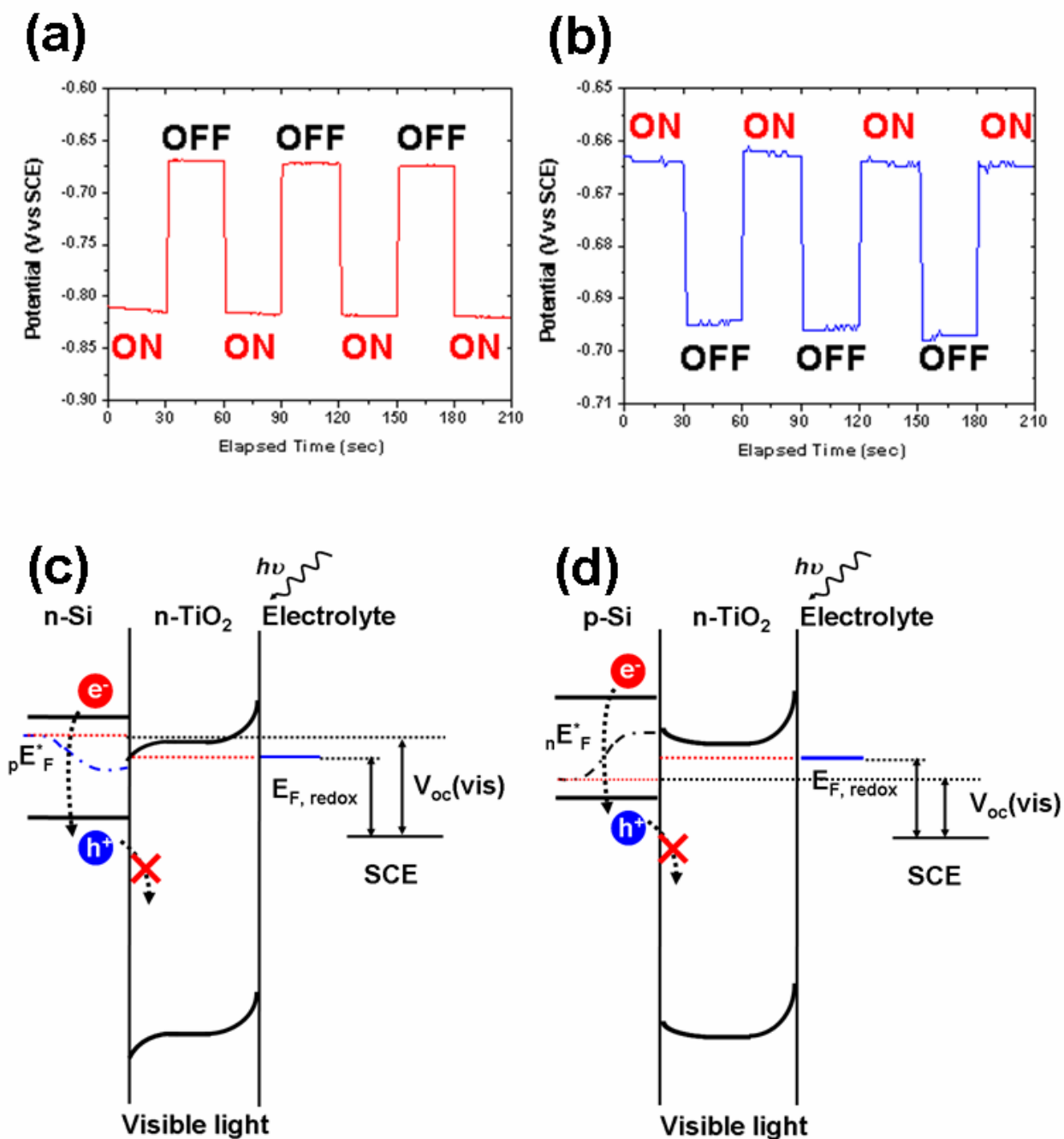


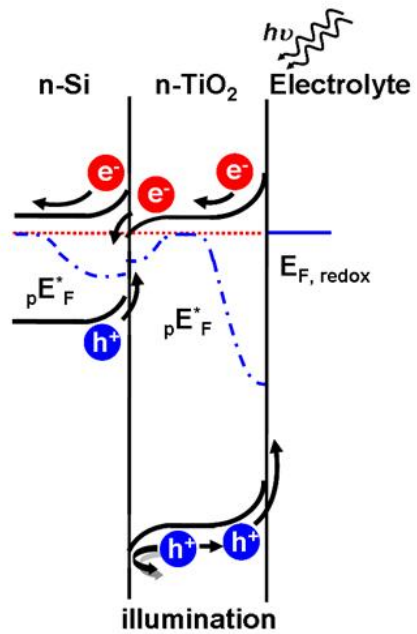
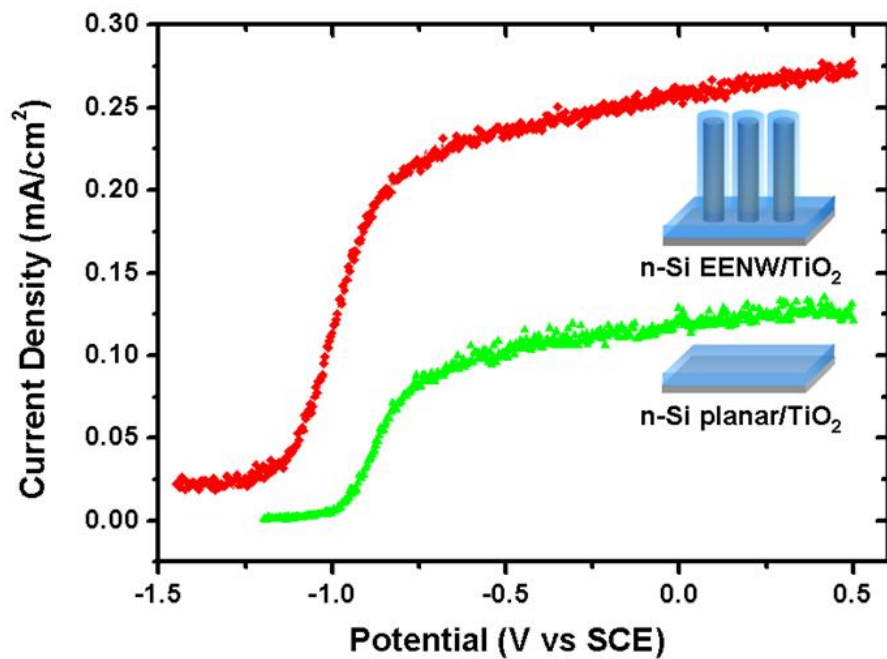
Figure 5. Open circuit voltage (V_{oc}) versus elapsed time for (a) n-Si EENW/TiO₂ and (b) p-Si EENW/TiO₂ arrays under visible light illumination (< 420 nm, ON) and in dark (OFF), and schematic diagram of band bending and V_{oc} for (c) n-Si EENW/TiO₂ and (d) p-Si EENW/TiO₂ arrays under visible light illumination, demonstrating that n-Si EENW/TiO₂ increase V_{oc} the while the p-Si EENW/TiO₂ decrease the V_{oc} under visible light.

References

- (1) Lewis, N. S.; Nocera, D. G. *Proc. Natl. Acad. Sci. USA* **2006**, *103*, 15729.
- (2) Sanderson, K. *Nature* **2008**, *452*, 400.
- (3) Grätzel, M. *Nature* **2001**, *414*, 338.
- (4) Nowotny, J.; Sorrell, C. C.; Sheppard, L. R.; Bak, T. *Int. J. Hydrogen. Energy* **2005**, *30*, 521.
- (5) Fujishima, A.; Honda, K. *Nature* **1972**, *238*, 37.
- (6) Rajeshwar, K. *J. Appl. Electrochem.* **2007**, *37*, 765.
- (7) Ni, M.; Leung, M.K.; Leung, D. Y.; Sumathy, K. *Renewable & Sustainable Energy Reviews* **2007**, *11*, 461.
- (8) Kitano, M.; Matsuoka, M.; Ueshima, M.; Anpo, M. *Appl. Catalysis A* **2007**, *325*, 1.
- (9) Park, J. H.; Kim, S.; Bard, A. J. *Nano. Lett.* **2005**, *6*, 24.
- (10) Kongkanad, A.; Dominguez, R. M.; Kamat, P.V *Nano. Lett.* **2007**, *7*, 676.
- (11) Kavan, L.; Grätzel, M.; Gilbert, S.E.; Klemenz, C.; Scheel, H. J. *J. Am. Chem. Soc.* **1996**, *118*, 6716.
- (12) Takabayashi, S.; Nakamura, R.; Nakato, Y. *J. Photochem. Photobiol. A* **2004**, *166*, 107.
- (13) Morisaki, H.; Watanabe, T.; Iwase, M.; Yazawa, K. *Appl. Phys. Lett.* **1976**, *29*, 338.
- (14) Lin, C. Y.; Fang, Y. K.; Kuo, C. H.; Chen, S. F.; Lin, C.; Chou, T. H.; Lee, Y.; Lin, J.; Hwang, S. *Appl. Surf. Sci.* **2006**, *253*, 898.
- (15) Khaselev, O.; Turner, J. A. *Science* **1998**, *280*, 425.
- (16) Yin, Y.; Jin, Z.; Hou, F. *Nanotechnology* **2007**, *18*, 495608.
- (17) Yu, Z. G.; Pryor, C. E.; Lau, W. H.; Berding, M. A.; MacQueen, D. B. *J. Phys. Chem. B.* **2005**, *109*, 22913.
- (18) Mor, G. K.; Vargnese, O. K.; Wilke, R. H.; Sharma, S.; Shankar, K.; Latempa, T.; Choi, K.; Grimes, C. A. *Nano. Lett.* **2008**, *8*, 3555.
- (19) Gerischer, H. *Solar Energy Conversion*; Springer Berlin: Heidelberg, 1979; p115-172.
- (20) Wagner, S.; Shay, J. L.; *Appl. Phys. Lett.* **1977**, *31*, 446.

- (21) Hovel, H. J.; Woodall, J. M.; *J. Electrochem. Soc.* **1973**, *120*, 1246.
- (22) Peng, K. Q.; Xu, Y.; Wu, Y.; Yan, Y. J.; Lee, S. T.; Zhu, J. *Small* **2005**, *1*, 1062.
- (23) Radecka, M.; Rekas, M.; Trenczeck-Zajac, A.; Zakrzewska, K. *J. Power. Sources.* **2008**, *181*, 46.
- (24) Mahajan, V. K.; Misra, M.; Raja, K. S.; Mohapatra, S.K.; *J. Phys. D: Appl. Phys.* **2008**, *41*, 125307.
- (25) Akiknsa, Jun.; Khan, S. U.; *Int. J. Hydrogen. Energy.* **1997**, *22*, 875.
- (26) Cheng, H.; Lee, W.; Hsu, C.; Hon, M.; Huang, C. *Electrochem. Solid-State. Lett.* **2008**, *11*, D81.
- (27) Bard, A. J.; Faulkner, L. R. *Electrochemical Methods: Fundamentals and Applications*; John Wiley & Sons, Inc.: New York, 1980; p637.
- (28) Bak, T.; Nowotny, J.; Rekas, M.; Sorrell, C. C. *Int. J. Hydrogen. Energy* **2002**, *27*, 991.
- (29) Perego, M.; Seguíni, G.; Scarel, G.; Fanciulli, M.; Wallrapp, F. *J. Appl. Phys.* **2008**, *103*, 43509.
- (30) Asahi, R.; Taga, Y.; Mannstadt, W.; Freeman A. J. *Phys. Rev. B.* **2000**, *61*, 7459.
- (31) Sze, S. M. *Physics of Semiconductor Devices*; John Wiley & Sons, Inc.: New York, 1981; p790-825.
- (32) Nelson, J. *The Physics of Solar Cell*; Imperial College Press.: London, 2002; p276.
- (33) Hinckley, S.; Mccann, J. F.; Haneman, D. *Solar Cells* **1986**, *17*, 317

SYNOPSIS TOC (Word Style "SN_Synopsis_TOC").



DISCLAIMER

This document was prepared as an account of work sponsored by the United States Government. While this document is believed to contain correct information, neither the United States Government nor any agency thereof, nor The Regents of the University of California, nor any of their employees, makes any warranty, express or implied, or assumes any legal responsibility for the accuracy, completeness, or usefulness of any information, apparatus, product, or process disclosed, or represents that its use would not infringe privately owned rights. Reference herein to any specific commercial product, process, or service by its trade name, trademark, manufacturer, or otherwise, does not necessarily constitute or imply its endorsement, recommendation, or favoring by the United States Government or any agency thereof, or The Regents of the University of California. The views and opinions of authors expressed herein do not necessarily state or reflect those of the United States Government or any agency thereof or The Regents of the University of California.